Weicheng Huang
School of Mechanical Engineering,
Southeast University,
Nanjing 211189, China;
Jiangsu Engineering Research Center of
Aerospace Machinery,
Southeast University,
Nanjing 211189, China
e-mail: weichenghuang@seu.edu.cn

Longhui Qin
School of Mechanical Engineering,
Southeast University,
Nanjing 211189, China
e-mail: lhqin@seu.edu.cn

Qiang Chen[1]
School of Mechanical Engineering,
Southeast University,
Nanjing 211189, China;
Jiangsu Engineering Research Center of
Aerospace Machinery,
Southeast University,
Nanjing 211189, China
e-mail: qiangchen@seu.edu.cn

Numerical Exploration on Snap Buckling of a Pre-Stressed Hemispherical Gridshell

Motivated by the observations of snap-through phenomena in pre-stressed strips and curved shells, we numerically investigate the snapping of a pre-buckled hemispherical gridshell under apex load indentation. Our experimentally validated numerical framework on elastic gridshell simulation combines two components: (i) discrete elastic rods method, for the geometrically nonlinear description of one-dimensional rods, and (ii) a naive penalty-based energy functional, to perform the non-deviation condition between two rods at joint. An initially planar grid of slender rods can be actuated into a three-dimensional hemispherical shape by loading its extremities through a prescribed path, known as buckling-induced assembly; next, this pre-buckled structure can suddenly change its bending direction at some threshold points when compressing its apex to the other side. We find that the hemispherical gridshell can undergo snap-through buckling through two different paths based on two different apex loading conditions. The structural rigidity increases as the number of rods in the gridshell structure becomes denser, which emphasizes the mechanically nonlocal property in hollow grids, in contrast to the local response of continuum shells. The findings may bridge the gap among rods, grids, knits, and shells, for a fundamental understanding of a group of thin elastic structures, and inspire the design of novel micro-electro-mechanical systems and functional metamaterials.
[DOI: 10.1115/1.4052289]

Keywords: computational mechanics, elasticity, structures

1 Introduction

Elastic gridshells are a class of net-like structures formed by an ensemble of elastically deforming rods coupled through joint points, which allow them to cover large span with low self-weight and serve for both structural and esthetical purposes in civil engineering community [1], e.g., Centre Pompidou Metz, Yas Hotel, and Helsinki Zoo's Observatory Tower. Besides the construction of buildings [2–4], some interesting applications in engineering structures, e.g., micro/nano structures [5–7], stretchable electronics [8,9], and bio-inspired patterns [10,11], also harness gridshells as their major structural components in the design step to achieve specific functionalities. Particularly, elastic gridshells fit the recent trend in extreme mechanics to the design of three-dimensional (3D) structures through buckling instability by utilizing its geometric uniqueness [12], i.e., a two-dimensional (2D) planar gridshell can undergo buckling instability and be actuated into 3D shell-like structure by compressing its boundary nodes [13,14]. This type of mechanically guided assembly of elastic structures has excellent compatibility and broad applicability to a variety of material properties and different length scales [12,15,16].

On the other side, the bending direction of the pre-stressed 3D gridshell can suddenly reverse when compressive load is applied at its apex, known as "snap-through buckling." Similar swift transformation process between multiple stable configurations in response to external stimuli exists in both artificial and natural systems, including toy poppers [17], soft robotics [18], Venus flytrap [19], and slap bracelet [20]. Previous investigations on snap buckling mainly focus on a single rod/ribbon-like system under different loading and boundary conditions, e.g., asymmetrical constraints [21,22], stretching [23,24], twisting [25], shearing [26], and out-of-plane compression [27,28], while the systematic investigations on the multi-stability and the complex configurations of multiple rods structure are quite limited [29,30]. Moreover, even though the buckling instability and shape shifting of 2D curved surfaces like cylinders [31–34] and spheres/hemispheres [31,35–43] have been largely studied, the buckling patterns in hollow gridshells would be different from the ones in continuum spherical shells [37,38]. The nonlinear responses of reticulated domes, e.g., stability, buckling, and snapping, have also drawn tremendous attention to the researchers in the structural mechanics community [44–46].

Inspired by the snapping in both 1D strips and 2D shells, we numerically study the snap-through buckling and the symmetry breaking of a pre-stressed hemispherical gridshell under apex load indentation. The geometrically nonlinear deformation of each rod in the gridshell structure is individually captured by the well-established discrete elastic rods (DERs) method [47–49]; a stiff spring is later introduced to simulate the mechanics of the joint between two rods through an explicit approach [13,50,51]. Excellent agreements between experiments and simulations have been found during the investigations of form finding [13] and rigidity measurement [14] in elastic gridshell structures. Also, quite recently, Romero et al. quantitatively verified these computer graphics simulators through extensive experiments to show the success of discrete differential geometry (DDG)-based frameworks in engineering problems [52]. Here, supported by this experimentally validated framework and the form finding process of hemispherical gridshell [13,50,51], the snap-through buckling of a pre-stressed hemispherical gridshell under apex load indentation is investigated exhaustively. Figure 1 presents the numerical setup used in the current study. We find that the hemispherical gridshells can undergo snapping through two different paths with two different apex loading conditions: a "simply supported"-like loading (seeing Movie S1) and a "clamped"-like indentation (referring to Movie S2). The dependence of structural rigidity and critical snapping points on the number of rods in elastic gridshells is next measured. Similar to the previous study [14], we find all rods contribute to the rigidity of an elastic gridshell, which highlights the importance of structural nonlocality in hollow grids, in contrast to the local response in continuum shells [38]. Reference [13] mainly

[1]Corresponding author.
Manuscript received June 16, 2021; final manuscript received August 25, 2021; published online September 21, 2021. Assoc. Editor: Pedro Reis.

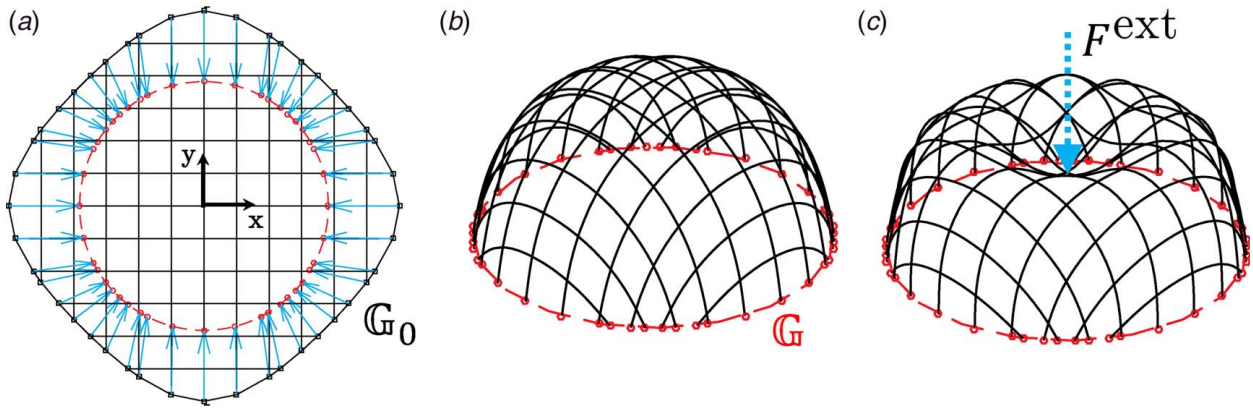

Fig. 1 Numerical setup. (*a*) The initial planar footprints and their corresponding trajectories for a buckling-induced hemispherical gridshell. (*b*) The deformed configuration of a pre-buckled hemispherical gridshell. (*c*) Apex indentation for a snap-through procedure.

considered the form finding process of an elastic gridshell, while paying only a little attention to its post-buckling behavior; Ref. [14] turned their focus to the studying of the post-buckling performance, e.g., rigidity of the whole structure, while the force–displacement curves and the mechanical responses are within a linear regime. Here, we focus on the nonlinear performance in gridshell's post-buckling regime. Moreover, the boundary conditions are different from the previous rigidity measurements. The structural rigidity investigated by Ref. [14] was from a clamped-like boundary condition, while the interesting snapping behavior could not be found during this type of asymmetrical boundary conditions. The footprints considered here are symmetric "pin–pin"-like boundary conditions, thus the snap-through between the bistable patterns could be observed. Overall, the rich behaviors and complex configurations in hemispherical gridshell under apex loading indentation would bridge the gaps among a group of thin elastic structures, e.g., rods [47–49], grids [13,14,50,51,53], knits [54–57], and shells [31,38,58,59], and motivate novel design of advanced micro-electro-mechanical systems and functional structures, e.g., a tether-net for the capture of space targets [60,61].

The rest of the paper is organized as follows. In Sec. 2, we introduce the numerical framework for the simulation of elastic gridshells. Next, in Sec. 3, the buckling-induced shape construction of hemispherical gridshell is briefly reviewed, followed by a detailed discussion on its snap-through buckling under apex loading. Finally, conclusive remarks and the potential opportunities for future research directions are summarized in Sec. 4.

2 Numerical Method

In this section, we discuss the numerical framework of elastic gridshell simulation. A description of DER is provided in Sec. 2.1 [47–49], and its extension to gridshell simulation is in Sec. 2.2, which was originally proposed by Baek et al. [13,14].

2.1 Discrete Elastic Rods Method. We use the DER method [47–49] to model the geometrically nonlinear deformation of thin rods. The rod centerline is first discretized into N nodes and $N-1$ segments, such that the edge vector is the difference between two consecutive nodes, $\mathbf{e}^i = \mathbf{x}_{i+1} - \mathbf{x}_i$, with $i \in [0, 1, \ldots, N-2]$. In our DER framework, the subscripts are used to denote the quantities associated with nodes, e.g., $\mathbf{x}_i$, and superscripts are for the quantities associated with edges, e.g., $\mathbf{e}^i$. Each edge, $\mathbf{e}^i$, has two orthonormal frames: (i) reference frame $\{\mathbf{d}_1^i, \mathbf{d}_2^i, \mathbf{t}^i\}$ and (ii) material frame $\{\mathbf{m}_1^i, \mathbf{m}_2^i, \mathbf{t}^i\}$; both of the frames share the tangent $\mathbf{t}^i = \mathbf{e}^i/\|\mathbf{e}^i\|$ as one of the directors. The twisting angle between two frames at the ith edge is defined as θ^i, refer to Fig. 2(*a*). The overall configuration of a discrete 1D structure can be thoroughly described by nodal positions, $\mathbf{x}_i$, as well as twisting angles, θ^i; and, as a result,

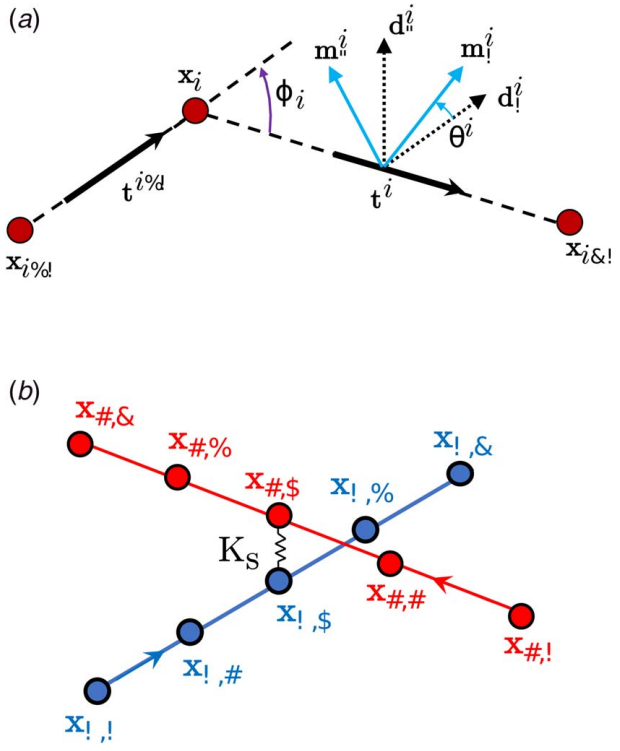

Fig. 2 (*a*) Notations used in the DER model and (*b*) Geometric decomposition between two connected rods in an elastic gridshell. The geometric decomposition is identical to the one used in Ref. [13].

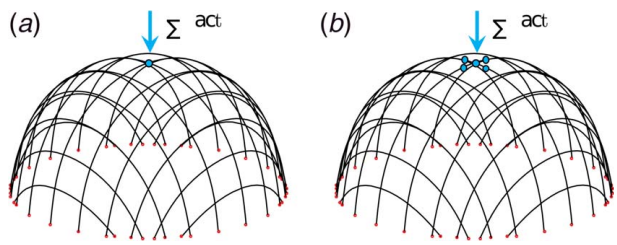

Fig. 3 Diagram of boundary and apex loading conditions. (*a*) "Simply supported"-like (mode I) loading process and (*b*) "Clamped"-like (mode II) loading process.

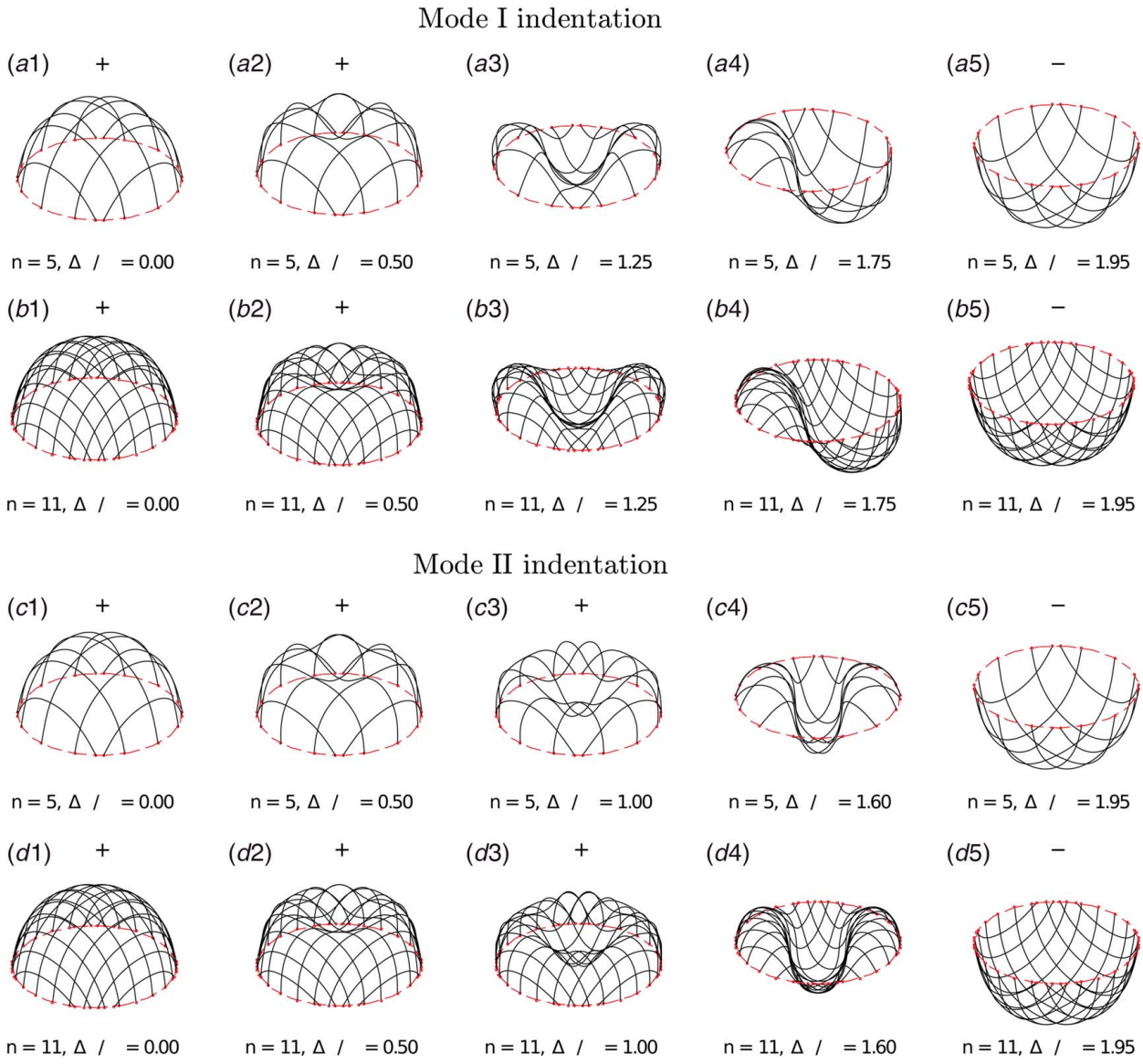

Fig. 4 Snapshots of pre-deformed hemispherical gridshells at different apex displacements. (*a*) and (*b*) "Simply supported"-like loading condition (mode I). (*c*) and (*d*) "Clamped"-like loading condition (mode II). The rod numbers are $n \in \{5, 11\}$, separately; the apex displacements for (*a*) and (*b*) are $\Delta D/R \in \{0.00, 0.50, 1.25, 1.75, 1.95\}$, and the apex displacements for (*c*) and (*d*) are $\Delta D/R \in \{0.00, 0.50, 1.00, 1.60, 1.95\}$.

a $4N-1$ sized degrees-of-freedom (DOF) vector, $\mathbf{q} = [\mathbf{x}_0, \theta^0, \mathbf{x}_1, \ldots, \mathbf{x}_{N-2}, \theta^{N-2}, \mathbf{x}_{N-1}]^T$, is constructed to capture the shape of a single rod system.

An elastic rod is treated as a mass-spring system, with a lumped mass (and angular mass) at each node (and edge) and associated discrete stretching, bending, and twisting energies. For a rod with Young's modulus E, shear modulus G, and isotropic circular cross section, the elastic energies—stretching, bending, and twisting—are given by [47,48]

$$E_s = \frac{1}{2}\sum_{i=0}^{N-2} EA(\epsilon^i)^2 \|\bar{\mathbf{e}}^i\| \tag{1a}$$

$$E_b = \frac{1}{2}\sum_{i=0}^{N-1} EI\left[(\kappa_i^{(1)} - \bar{\kappa}_i^{(1)})^2 + (\kappa_i^{(2)} - \bar{\kappa}_i^{(2)})^2\right]\Delta l_i \tag{1b}$$

$$E_t = \frac{1}{2}\sum_{i=0}^{N-1} GJ(\tau_i)^2 \Delta l_i \tag{1c}$$

where A is the area of cross section, I is the bending moment of inertia, J is the polar moment of inertia, ϵ^i is the discrete stretching strain associated with the ith edge, $\kappa_i^{(1)}$ and $\kappa_i^{(2)}$ are the discrete bending curvatures at the ith node ($\bar{\kappa}_{1,i}$ and $\bar{\kappa}_{2,i}$ are the curvatures in the undeformed configuration), τ_i is the twist at the ith node, $\bar{\mathbf{e}}^i$ is the undeformed length of ith edge, and $\Delta l_i = \left(\|\bar{\mathbf{e}}^i\| + \|\bar{\mathbf{e}}^{i+1}\|\right)/2$ is the Voronoi length at ith vertex. The strain measures, i.e., ϵ^i, $\kappa_i^{(1)}$, $\kappa_i^{(2)}$, and τ_i, can be expressed in terms of $\mathbf{q}$. Details can be found in Refs. [47–49].

A first order, implicit Euler integration is used to solve the equations of motion and update the DOF vector, $\mathbf{q}$, as well as its velocity, $\mathbf{v} \equiv \dot{\mathbf{q}}$, from time-step t_k to $t_{k+1} = t_k + h$ (h is the time-step size) [62]:

$$\mathbb{M}\Delta\mathbf{q}_{k+1} - h\mathbb{M}\mathbf{v}_k - h^2\left(\mathbf{F}_{k+1}^{\text{int}} + \mathbf{F}_{k+1}^{\text{ext}}\right) = \mathbf{0} \tag{2a}$$

$$\mathbf{q}_{k+1} = \mathbf{q}_k + \Delta\mathbf{q}_{k+1} \tag{2b}$$

$$\mathbf{v}_{k+1} = \frac{1}{h}\Delta\mathbf{q}_{k+1} \tag{2c}$$

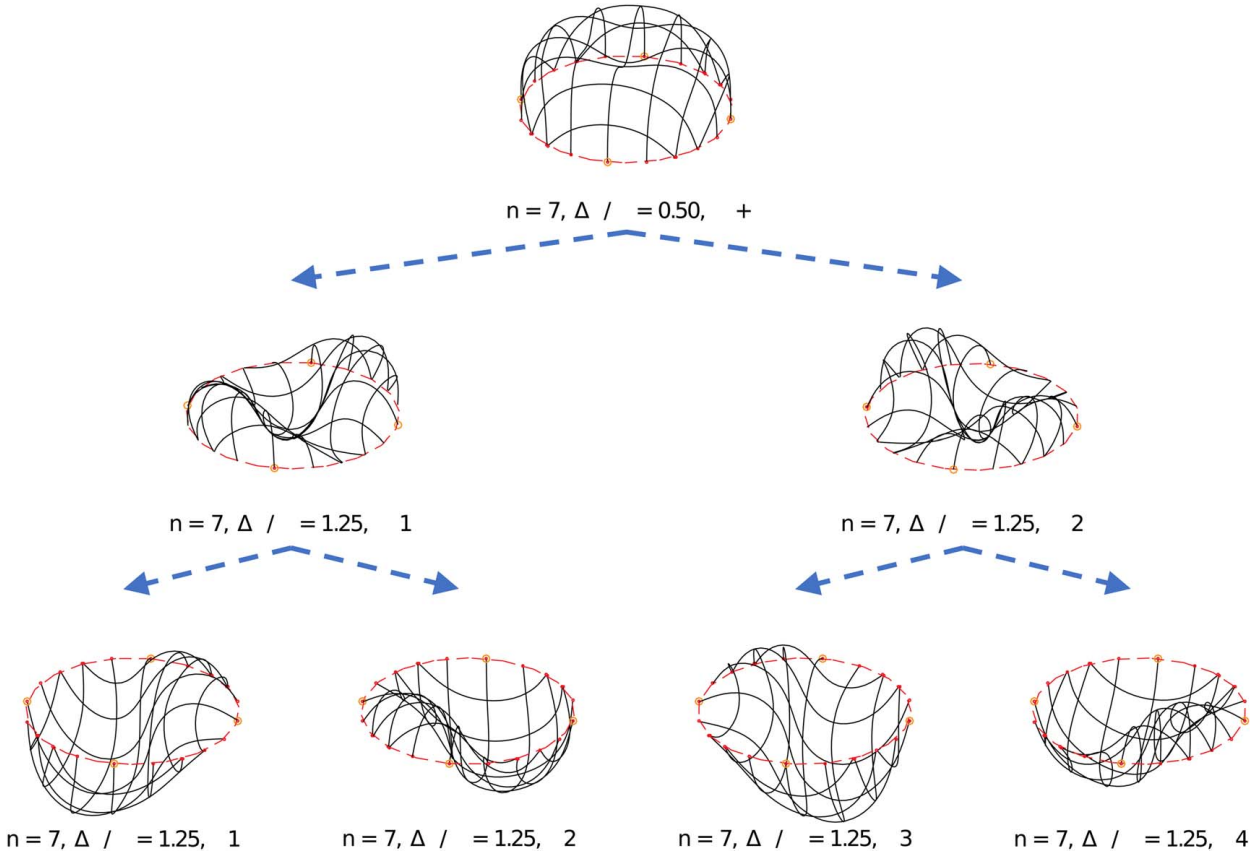

Fig. 5 Symmetry breaking of a hemispherical gridshell under apex indentation. Here, the apex indentation is a "simply supported"-like loading condition (mode I), and the rod number is $n = 7$. The footprints of two longest rods are marked as dots.

where $\mathbf{F}^{\text{int}}$ is the internal elastic force vector, $\mathbf{F}^{\text{ext}}$ is the external force vector (e.g., gravity, damping, and actuation force), $\mathbb{M}$ is the diagonal mass matrix composed of the lumped masses [62], and the superscript $k+1$ (and k) denotes evaluation of the quantities at time t_{k+1} (and t_k). Newton's method is used to iteratively optimize the DOF vector until the error is within the tolerance. Even though this method is originally developed for the dynamic simulation of mechanical systems, the equilibrium configurations of structures can be eventually obtained with damping forces added into the system, known as the dynamic relaxation method. Moreover, as the inertial effect is included, this framework can automatically capture the symmetry breaking between the stable and the unstable phases by introducing some imperfections or perturbations [63].

2.2 Discrete Elastic Gridshell Simulation. Now we formulate the discrete numerical framework for the simulation of gridshells, which was identical to the method used in Refs. [13,14]. We consider a basic element of gridshell structure in Fig. 2(*b*), where two rods intersect each other at a shared joint. The position of the *j*th node on the *i*th rod within the gridshell system is denoted as $\mathbf{x}_{i,j}$. Here, $\mathbf{x}_{0,2}$ and $\mathbf{x}_{1,2}$ are overlapped at the joint point. A straightforward method to enforce the coincidence of two nodes at the joint is a linear spring-like penalty energy of the form

$$E_c = \frac{1}{2} K_s \|\mathbf{x}_{0,2} - \mathbf{x}_{1,2}\|^2 \tag{3}$$

where K_s performs like a Lagrange multiplier. Its negative gradient, $-\partial E_c/\partial \mathbf{q}$, is included as an external force in Eq. (2*a*). The final result shows good convergence as the increasing of the spring stiffness K_s [13,14,50,51]. In our study, we limit our scope to joints with positional constraints but ignore the bending and twisting coupling [51,53,64], in order to increase the flexibility of the gridshell system.

3 Results

In this section, we first briefly discuss how to utilize buckling instability to construct a 3D hemispherical gridshell from an initial planar grid of rods, then study its snap-through phenomenon under apex loading indentation.

3.1 Form Finding of Hemispherical Gridshell. The geometrical and physical parameters in the current numerical study are: rod number $2n \in \{10, 14, 18, 22\}$, rod radius $r_0 = 1$ mm (and, therefore, second moment of inertia $I = \pi r_0^4/4$, polar moment of inertia $J = \pi r_0^4/2$, and cross-sectional area $A = \pi r_0^2$), Young's modulus $E = 100$ GPa, shear modulus $G = E/3$ (assuming incompressible material), and material density $\rho = 1000$ kg/m^3. The hemispherical diameter is $2R = 7.64$ cm, resulting in its half-span (as well as the length of longest rods in gridshell) $L = 12.00$ cm and its nodal number $N \approx 120$. As this is a geometry dependent problem, negligible variations are found when changing the material-related parameters, e.g., Young's modulus and density. The boundary nodes, $\{\mathbf{x}_{i,0}, \mathbf{x}_{i,N-1}\}$, as well as the boundary angles, $\{\theta^{i,0}, \theta^{i,N-2}\}$, for all rods (with $i \in [0, 1, 2, \ldots, 2n-1]$) are constrained to achieve the pin–pin boundary conditions. Specifically, the boundary nodes are manually moved along a prescribed path (shown in Fig. 1(*a*)) with an extremely low speed, $v_{bc} = 1$ mm/s, in order to avoid inertial effect and higher order dynamic buckling modes; the boundary angles, on the other hand, are fixed as zeros all the time to avoid rigid body rotations. After a convergence study, the discrete Voronoi length is $\Delta l = 1$ mm for gridshells composed of different numbers of rods, and the discrete time-step is set to be $h = 1$ ms.

The presented numerical framework can predict the deformed configuration of elastic gridshell under any given external actuation, while the inverse process, i.e., finding the initial planar configuration from a given 3D pattern, is also nontrivial. References

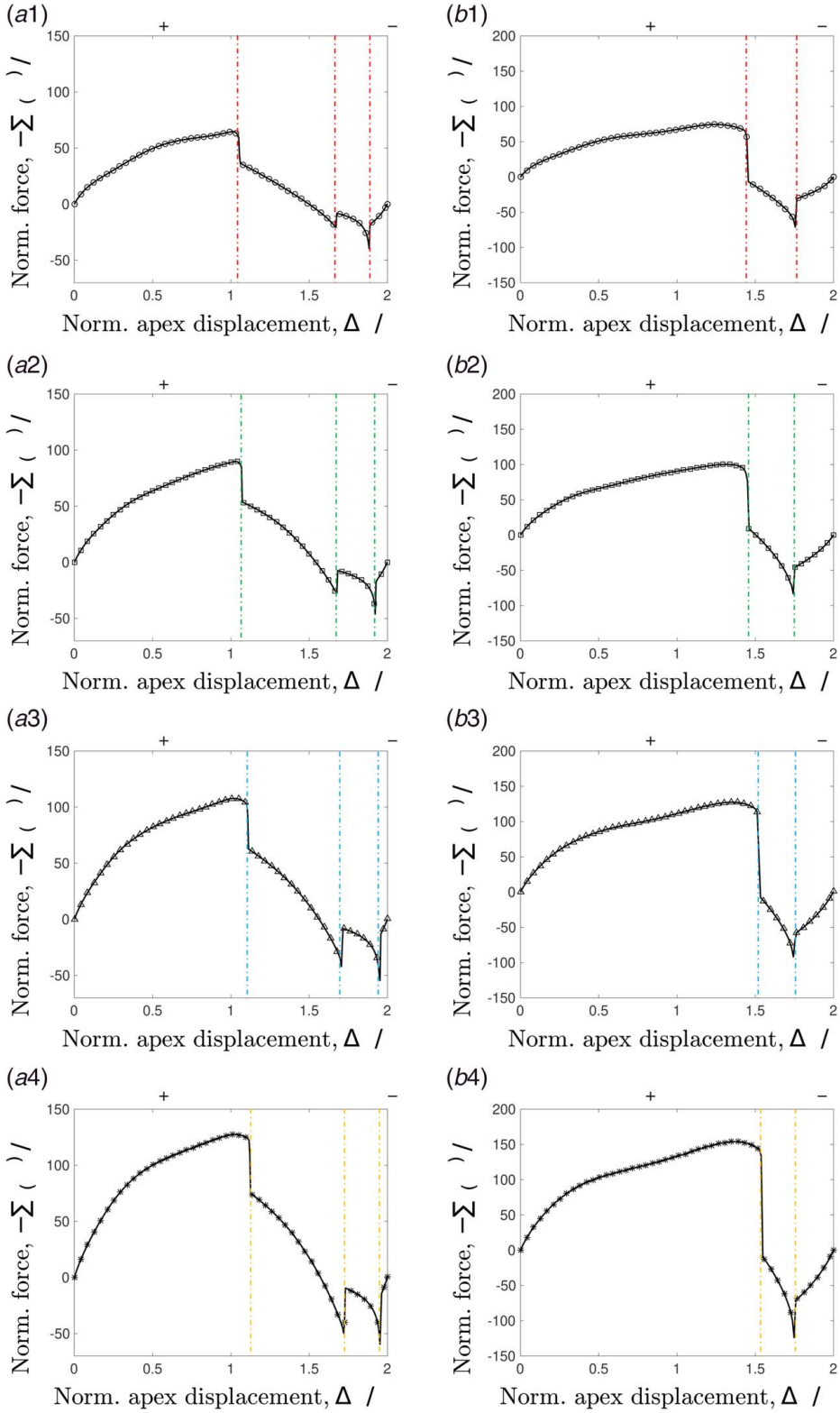

Fig. 6 Normalized external force as a function of normalized apex displacement for a hemispherical gridshell composed of different number of rods: (1)–(4) $n \in \{5, 7, 9, 11\}$. (*a*1)–(*a*4) "simply supported" like loading process (mode I). (*b*1)–(*b*4) "Clamped"-like loading process (mode II).

[13,14] adopted the theory of smooth Chebyshev nets to find the shape of the initially planar grid of rods and its corresponding trajectories on footprints, $\mathbb{G}_0 \Rightarrow \mathbb{G}$. Chebyshev's hemisphere is constructed by mapping the planar orthogonal coordinate system, (u, v), to the 3D hemisphere under inextensibility constraints, and the initial planar boundary can be numerically obtained through the integration of Gauss equation [13,65]. With a prescribed planar shape, $\mathbb{G}_0$, and specific trajectories of its extremities, shown in Fig. 1(*a*), a perfect hemispherical gridshell illustrated in Fig. 1(*b*) can be constructed. Details of the form finding process

for hemispherical gridshells can be found in the Supporting Information Appendix of Ref. [13]. The data-based form finding method and the contact-based form finding procedure are presented in Ref. [50] and Ref. [51], respectively.

3.2 Snap-Through Buckling. With the numerical framework and hemispherical gridshell constructed beforehand, we now turn to the main contribution of the current study and investigate its snap-through buckling under apex loading. In Fig. 3(*a*), we consider a pre-buckled hemispherical gridshell constructed by $2n = 22$ rods, and its footprints, marked as small dots, are constrained, resulting a simply supported boundary condition at the equator, which is identical to the boundary conditions used in Sec. 3.1. Dirichlet boundary condition is next introduced to specify the position of its apex, marked as blue dot, to perform the external loading, i.e., a positional constraint is applied onto the mechanical system and the required actuation force, $\mathbf{F}^{\text{act}} \equiv [F_x, F_y, F_z]^T$, is later evaluated from the statement of force balance. Because the hemispherical gridshell is constructed from a planar grid of rods, the intrinsic curvatures of the pre-deformed rods are zeros, $\bar{\kappa}_i^{(1)} = 0$, $\bar{\kappa}_i^{(2)} = 0$. Note that there are two constrained nodes at the top, i.e., one is on the longest rod parallel to *x*-axis, and the other is on the longest rod parallel to *y*-axis. All other nodes and edges are free to evolve based on the balance between the elastic and external forces. To totally avoid inertia effect, the reaction forces are derived when the system is in equilibrium; some small but finite perturbations are also included in our framework to induce the symmetry breaking and to find the stable equilibrium configurations of elastic gridshells.

The pre-buckled hemispherical gridshell would experience a complex shape transformation when its apex thrusts to the other side: an initially *U*+ shaped hemispherical gridshell, referring to Fig. 4, first transitions into the *O*+ configuration as the apex load increases; however, it suddenly switches to the *W* configuration at the first threshold snapping point, $\Delta D/R \approx 1.1$; here, ΔD is the apex displacement along the negative *z*-axis; next, the *W* pattern changes to the *S* shape at the second snapping point, $\Delta D/R \approx 1.7$. After that, with increasing apex displacement, the asymmetrical *S* form would shift to *O*− at $\Delta D/R \approx 1.9$, and finally goes into *U*-pattern when $\Delta D = 2R$. Also, as we expected, the rigidity of elastic gridshells increases as the structure becomes denser [14]. The corresponding configurations are shown in Figs. 4(*a*) and 4(*b*), and a representative video for $n = 11$ is provided in Movie S1. Note that at the first and the second snapping points, symmetry breaking phenomena is observed, i.e., there exists several different *W* and *S* patterns that are symmetric to each other, see Fig. 5 for details. Here, the collision between two approaching rods was ignored. In Figs. 6(*a*1)–(*a*4), we plot the *z* component of normalized external loading, $-\sum F_z R^2/EI$, as a function of normalized apex displacement, $\Delta D/R$, where the external forces are from the sum of two overlapped nodes at apex. We can clearly find three critical snapping points in the loading–displacement curve, and the configurations of elastic gridshell can thus be divided into four patterns during the loading stage, $O+ \Rightarrow W \Rightarrow S \Rightarrow O-$. The critical snapping points for gridshells with different rod density, $n \in \{5, 7, 9, 11\}$, are almost negligible.

Previous external loading is applied through a "simply supported"-like boundary condition (mode I), i.e., we only specify the apex position while its rotational angle is free. Here, we constrained six nodes, e.g., apex and its neighboring nodes, as shown in Fig. 3(*b*), such that a "clamped"-like boundary condition (mode II) can be achieved, e.g., both the position and the rotational angle at the apex are specified. A different snap-through buckling process is observed in this case, see Figs. 4(*c*) and 4(*d*) for details. Similar to the previous study, an initial *U*+ shaped hemispherical gridshell first transitions into *O*+ configuration. However, unlike the first case, the first critical snapping point that transforming from *O*+ to *W* appears at $\Delta D/R \approx 1.50$; next, instead of the shift from *W* to *S*, the gridshell structure directly jumps from *W* to *O*− at the second critical snapping point, $\Delta D/R \approx 1.75$; finally, *U*-configuration is obtained at $\Delta D/R = 2.00$ in a manner similar to the previous case. Because of the constraints in the rotational angle at apex, the unsymmetrical *S* pattern does not appear during the loading process. Figures 6(*b*1)–(*b*4) present the evolution of the *z* component of normalized loading with the normalized apex position for the mode II loading condition. Here, the total external loading is the sum of the forces applied on six nodes at apex. Two critical snapping points are observed in the loading–displacement curve, and the patterns of elastic gridshell are segregated into three phases, $O+ \Rightarrow W \Rightarrow O-$. A representative video for $n = 11$ is provided in Movie S2. Again, the critical snapping points for gridshells with different rod densities are insignificant.

Moving forward, in Fig. 7(*a*), we plot the dependence of the first critical snapping point on the number of rods, $n \in \{5, 7, 9, 11, 19, 29, 39, 49\}$. Here, for a general comparison, a denser gridshell was also considered. Even quite trivial, the first critical snapping point—the jump between *O*+ pattern and *W* configuration—slightly increases as the gridshell becomes denser when the structure is coarse (when $n \in \{5, 7, 9, 11\}$), for both mode I actuation (with $\Delta\tilde{D}/R \approx 1.1$) and mode II (with $\Delta\tilde{D}/R \approx 1.5$) indentation; however, the threshold snapping points show almost no variations when the number of rods changes from $n = 19$ to $n = 49$, which highlights the asymptotic behavior predicted by Ref. [14]. We do not find any governing law for other critical snapping points at this stage. In parallel, we perform the relations between the normalized maximum force in the force–displacement curve and the number of rods in Fig. 7(*b*). As expected, the rigidity of an elastic gridshell, which is related to the maximum external force, almost linearly increases as the enlargement of rod number, *n* [14].

For completeness, we perform a convergence study of discrete elastic gridshell simulation. Gridshell composed of $n \in \{5, 11\}$ rods is used for demonstration. In Fig. 8, we plot the force–displacement curves with different discrete Voronoi lengths, $\Delta l \in \{2.0, 1.5, 1.0, 0.5\}$ mm, for both (*a*1)–(*b*1) mode I indentation and

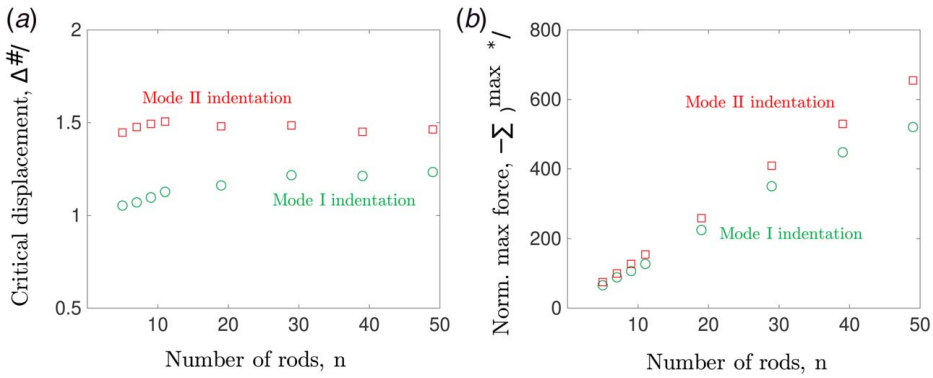

Fig. 7 (*a*) The dependence of the first snapping displacement on the number of rods in elastic gridshells and (*b*) Normalized maximum indentation force as a function of number of rods.

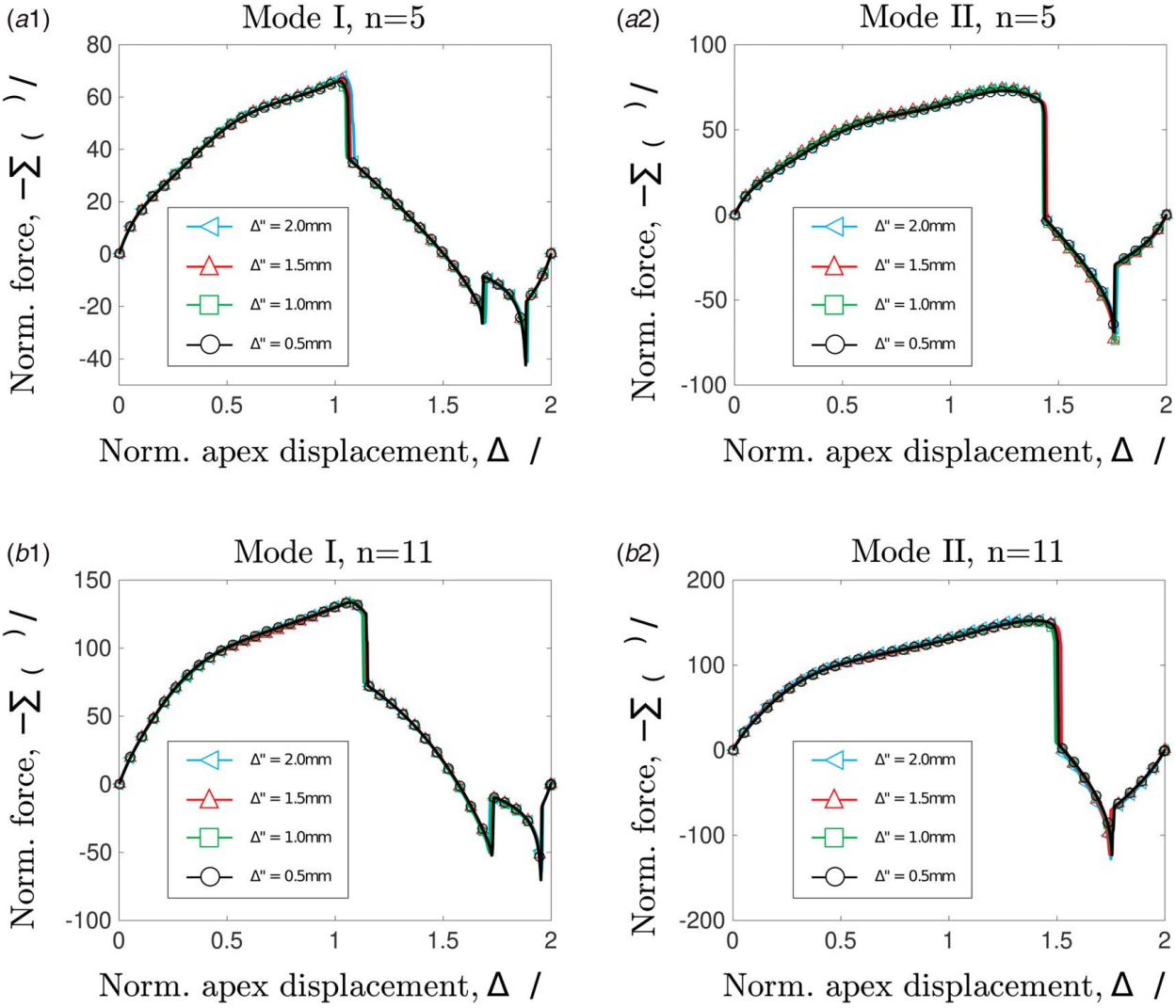

Fig. 8 Convergence study for (*a*1)–(*b*1) mode I indentation and (*a*2)–(*b*2) mode II indentation

(*a*2)–(*b*2) mode II condition. The overlapped curves indicate a good convergence of our discrete simulation.

4 Conclusion

In this paper, we numerically examined the snap-through behavior and the symmetry breaking of a pre-buckled hemispherical gridshell under apex load indentation. For this purpose, we employed an experimentally validated discrete model for the simulation of elastic gridshells. Our numerical framework is composed of two parts: (i) a well-established DER method for the geometrically nonlinear description of a single rod and (ii) a naive penalty-based constraint between two rods at joint. The inverse problem, finding the initial 2D undeformed configuration from a given hemispherical pattern, was evaluated by solving the Gauss equation on the basis of Chebyshev nets theory, which has already been solved and is not a novelty here. This pre-stressed hemispherical elastic would undergo a complicated shape transform and symmetry breaking when external load was applied onto its apex. Two different snap-through paths have been observed on the basis of different loading conditions. Moreover, we also found the structural rigidity showing an increasing trend as the number of rods in gridshell becomes denser, which differs from both 1D rod/ribbon-like structures and 2D plate/shell models. The structural stability, on the other side, first increases as the gridshell becomes denser, while shows almost no variations when the number of rods is large enough. On the other hand, we mainly limited ourselves to the "coarse" gridshell—the distance between two neighboring rods is significantly larger than rod radius. The snap-through phenomena of a "finer" net would be interesting for future research, e.g., finding a more general model that connects hollow gridshells, knitted structures, and continued shells. Future work may also involve some experimental investigations to verify the results presented in this paper. In closing, we hope that our numerical investigations can motivate a fundamental understanding of a group of thin elastic structures, as well as support modeling and design in advanced systems and functional materials.

Acknowledgment

We are grateful for the financial support from the Fundamental Research Funds for the Central Universities (No. 2242021R10024) and the Jiangsu Planned Projects for Postdoctoral Research Funds (2021K230B). We thank Changyeob Baek and Khalid Jawed for useful discussion.

Conflict of Interest

There are no conflicts of interest.

References

[1] Ghiyasinasab, M., Lehoux, N., and Ménard, S., 2017, "Production Phases and Market for Timber Gridshell Structures: A State-of-the-Art Review," BioResources, **12**(4), pp. 9538–9555.

[2] Quagliaroli, M., and Malerba, P., 2013, "Flexible Bridge Decks Suspended by Cable Nets. A Constrained Form Finding Approach," Int. J. Solids Struct., **50**(14–15), pp. 2340–2352.

[3] Tayeb, F., Caron, J.-F., Baverel, O., and Du Peloux, L., 2013, "Stability and Robustness of a 300 M2 Composite Gridshell Structure," Constr. Build. Mater., **49**, pp. 926–938.

[4] Lefevre, B., Douthe, C., and Baverel, O., 2015, "Buckling of Elastic Gridshells," J. Int. Assoc. Shell Spatial Struct., **56**(3), pp. 153–171.

[5] Li, Y., Song, J., Fang, B., and Zhang, J., 2011, "Surface Effects on the Postbuckling of Nanowires," J. Phys. D: Appl. Phys., **44**(42), p. 425304.

[6] Xu, S., Yan, Z., Jang, K.-I., Huang, W., Fu, H., Kim, J., Wei, Z., et al., 2015, "Assembly of Micro/Nanomaterials Into Complex, Three-Dimensional Architectures by Compressive Buckling," Science, **347**(6218), pp. 154–159.

[7] Zhao, H., Li, K., Han, M., Zhu, F., Vázquez-Guardado, A., Guo, P., Xie, Z., et al., 2019, "Buckling and Twisting of Advanced Materials Into Morphable 3D Mesostructures," Proc. Natl. Acad. Sci. U.S.A., **116**(27), pp. 13239–13248.

[8] Fan, J. A., Yeo, W.-H., Su, Y., Hattori, Y., Lee, W., Jung, S. -Y., Zhang, Y., et al., 2014, "Fractal Design Concepts for Stretchable Electronics," Nat. Commun., **5**, p. 3266.

[9] Jang, K.-I., Li, K., Chung, H. U., Xu, S., Jung, H. N., Yang, Y., Kwak, J. W., et al., 2017, "Self-Assembled Three Dimensional Network Designs for Soft Electronics," Nat. Commun., **8**, p. 15894.

[10] Jang, K.-I., Chung, H. U., Xu, S., Lee, C. H., Luan, H., Jeong, J., Cheng, H., et al., 2015, "Soft Network Composite Materials With Deterministic and Bio-Inspired Designs," Nat. Commun., **6**, p. 6566.

[11] Xu, Z., Fan, Z., Fu, H., Liu, Y., Zi, Y., Huang, Y., and Zhang, Y., 2019, "Optimization-Based Approach for the Inverse Design of Ribbon-Shaped Three-Dimensional Structures Assembled Through Compressive Buckling," Phys. Rev. Appl., **11**(5), p. 054053.

[12] Reis, P. M., Jiménez, F. L., and Marthelot, J., 2015, "Transforming Architectures Inspired by Origami," Proc. Natl. Acad. Sci. U.S.A., **112**(40), pp. 12234–12235.

[13] Baek, C., Sageman-Furnas, A. O., Jawed, M. K., and Reis, P. M., 2018, "Form Finding in Elastic Gridshells," Proc. Natl. Acad. Sci. U.S.A., **115**(1), pp. 75–80.

[14] Baek, C., and Reis, P. M., 2019, "Rigidity of Hemispherical Elastic Gridshells Under Point Load Indentation," J. Mech. Phys. Solids, **124**, pp. 411–426.

[15] Miller, J., Su, T., Dussan V, E. B., Pabon, J., Wicks, N., Bertoldi, K., and Reis, P., 2015, "Buckling-Induced Lock-Up of a Slender Rod Injected Into a Horizontal Cylinder," Int. J. Solids Struct., **72**, pp. 153–164.

[16] Filipov, E. T., Tachi, T., and Paulino, G. H., 2015, "Origami Tubes Assembled Into Stiff, Yet Reconfigurable Structures and Metamaterials," Proc. Natl. Acad. Sci. U.S.A., **112**(40), pp. 12321–12326.

[17] Pandey, A., Moulton, D. E., Vella, D., and Holmes, D. P., 2014, "Dynamics of Snapping Beams and Jumping Poppers," Europhys. Lett., **105**(2), p. 24001.

[18] Chen, T., Bilal, O. R., Shea, K., and Daraio, C., 2018, "Harnessing Bistability for Directional Propulsion of Soft, Untethered Robots," Proc. Natl. Acad. Sci. U.S.A., **115**(22), pp. 5698–5702.

[19] Forterre, Y., Skotheim, J. M., Dumais, J., and Mahadevan, L., 2005, "How the Venus Flytrap Snaps," Nature, **433**(7024), p. 421.

[20] Kebadze, E., Guest, S., and Pellegrino, S., 2004, "Bistable Prestressed Shell Structures," Int. J. Solids Struct., **41**(11–12), pp. 2801–2820.

[21] Gomez, M., Moulton, D. E., and Vella, D., 2017, "Critical Slowing Down in Purely Elastic 'Snap-Through' Instabilities," Nat. Phys., **13**(2), p. 142.

[22] Sano, T. G., and Wada, H., 2018, "Snap-Buckling in Asymmetrically Constrained Elastic Strips," Phys. Rev. E, **97**(1), p. 013002.

[23] Starostin, E., and van der Heijden, G., 2008, "Tension-Induced Multistability in Inextensible Helical Ribbons," Phys. Rev. Lett., **101**(8), p. 084301.

[24] Morigaki, Y., Wada, H., and Tanaka, Y., 2016, "Stretching an Elastic Loop: Crease, Helicoid, and Pop Out," Phys. Rev. Lett., **117**(19), p. 198003.

[25] Sano, T. G., and Wada, H., 2019, "Twist-Induced Snapping in a Bent Elastic Rod and Ribbon," Phys. Rev. Lett., **122**(11), p. 114301.

[26] Yu, T., and Hanna, J., 2019, "Bifurcations of Buckled, Clamped Anisotropic Rods and Thin Bands Under Lateral End Translations," J. Mech. Phys. Solids, **122**, pp. 657–685.

[27] Zhang, Y., Jiao, Y., Wu, J., Ma, Y., and Feng, X., 2020, "Configurations Evolution of a Buckled Ribbon in Response to Out-of-Plane Loading," Extreme Mech. Lett., **34**, p. 100604.

[28] Wan, G., Liu, Y., Xu, Z., Jin, C., Dong, L., Han, X., Zhang, J. X., and Chen, Z., 2020, "Tunable Bistability of a Clamped Elastic Beam," Extreme Mech. Lett., **34**, p. 100603.

[29] Malek, S., Wierzbicki, T., and Ochsendorf, J., 2014, "Buckling of Spherical Cap Gridshells: A Numerical and Analytical Study Revisiting the Concept of the Equivalent Continuum," Eng. Struct., **75**, pp. 288–298.

[30] Yu, T., Dreier, L., Marmo, F., Gabriele, S., Parascho, S., and Adriaenssens, S., 2021, "Numerical Modeling of Static Equilibria and Bifurcations in Bigons and Bigon Rings," J. Mech. Phys. Solids, **152**, p. 104459.

[31] Bende, N. P., Evans, A. A., Innes-Gold, S., Marin, L. A., Cohen, I., Hayward, R. C., and Santangelo, C. D., 2015, "Geometrically Controlled Snapping Transitions in Shells With Curved Creases," Proc. Natl. Acad. Sci. U.S.A., **112**(36), pp. 11175–11180.

[32] Pezzulla, M., Stoop, N., Jiang, X., and Holmes, D. P., 2017, "Curvature-Driven Morphing of Non-Euclidean Shells," Proc. R. Soc. A: Math. Phys. Eng. Sci., **473**(2201), p. 20170087.

[33] Jiang, X., Pezzulla, M., Shao, H., Ghosh, T. K., and Holmes, D. P., 2018, "Snapping of Bistable, Prestressed Cylindrical Shells," Europhys. Lett., **122**(6), p. 64003.

[34] Lavrenčič, M., and Brank, B., 2018, "Simulation of Shell Buckling by Implicit Dynamics and Numerically Dissipative Schemes," Thin-Walled Struct., **132**, pp. 682–699.

[35] Huang, N.-C., 1964, "Unsymmetrical Buckling of Thin Shallow Spherical Shells," ASME J. Appl. Mech., **31**(3), pp. 447–457.

[36] Huang, N. C., 1969, "Axisymmetric Dynamic Snap-Through of Elastic Clamped Shallow Spherical Shells," AIAA J., **7**(2), pp. 215–220.

[37] Vaziri, A., and Mahadevan, L., 2008, "Localized and Extended Deformations of Elastic Shells," Proc. Natl. Acad. Sci. U.S.A., **105**(23), pp. 7913–7918.

[38] Lazarus, A., Florijn, H., and Reis, P. M., 2012, "Geometry-Induced Rigidity in Nonspherical Pressurized Elastic Shells," Phys. Rev. Lett., **109**(14), p. 144301.

[39] Shim, J., Perdigou, C., Chen, E. R., Bertoldi, K., and Reis, P. M., 2012, "Buckling-Induced Encapsulation of Structured Elastic Shells Under Pressure," Proc. Natl. Acad. Sci. U.S.A., **109**(16), pp. 5978–5983.

[40] Marthelot, J., López Jiménez, F., Lee, A., Hutchinson, J. W., and Reis, P. M., 2017, "Buckling of a Pressurized Hemispherical Shell Subjected to a Probing Force," ASME J. Appl. Mech., **84**(12), p. 121005.

[41] Evkin, A., Kolesnikov, M., and Prikazchikov, D. A., 2017, "Buckling of a Spherical Shell Under External Pressure and Inward Concentrated Load: Asymptotic Solution," Math. Mech. Solids, **22**(6), pp. 1425–1437.

[42] Hutchinson, J. W., and Thompson, J. M. T., 2018, "Imperfections and Energy Barriers in Shell Buckling," Int. J. Solids Struct., **148**, pp. 157–168.

[43] Chen, T., Pauly, M., and Reis, P. M., 2021, "A Reprogrammable Mechanical Metamaterial With Stable Memory," Nature, **589**(7842), pp. 386–390.

[44] Gioncu, V., 1995, "Buckling of Reticulated Shells: State-of-the-Art," Int. J. Space Struct., **10**(1), pp. 1–46.

[45] Plaut, R. H., 2018, "Snap-Through of Shallow Reticulated Domes Under Unilateral Displacement Control," Int. J. Solids Struct., **148**, pp. 24–34.

[46] Guan, Y., Virgin, L. N., and Helm, D., 2018, "Structural Behavior of Shallow Geodesic Lattice Domes," Int. J. Solids Struct., **155**, pp. 225–239.

[47] Bergou, M., Wardetzky, M., Robinson, S., Audoly, B., and Grinspun, E., 2008, "Discrete Elastic Rods," ACM Trans. Graph., **27**(3), p. 63.

[48] Bergou, M., Audoly, B., Vouga, E., Wardetzky, M., and Grinspun, E., 2010, "Discrete Viscous Threads," ACM Trans. Graph., **29**, p. 116.

[49] Jawed, M. K., Novelia, A., and O'Reilly, O. M., 2018, *A Primer on the Kinematics of Discrete Elastic Rods*, Springer, Cham.

[50] Qin, L., Huang, W., Du, Y., Zheng, L., and Jawed, M. K., 2020, "Genetic Algorithm-Based Inverse Design of Elastic Gridshells," Struct. Multidiscipl. Optim., **62**(5), pp. 2691–2707.

[51] Huang, W., Qin, L., and Khalid Jawed, M., 2021, "Numerical Method for Direct Solution to Form-Finding Problem in Convex Gridshell," ASME J. Appl. Mech., **88**(2), p. 021012.

[52] Romero, V., Ly, M., Rasheed, A.-H., Charrondière, R., Lazarus, A., Neukirch, S., and Bertails-Descoubes, F., 2021, "Physical Validation of Simulators in Computer Graphics: A New Framework Dedicated to Slender Elastic Structures and Frictional Contact," ACM Trans. Graph.

[53] Panetta, J., Konaković-Luković, M., Isvoranu, F., Bouleau, E., and Pauly, M., 2019, "X-shells: A New Class of Deployable Beam Structures," ACM Trans. Graph., **38**(4), p. 83.

[54] Kaldor, J. M., James, D. L., and Marschner, S., 2008, "Simulating Knitted Cloth at the Yarn Level," ACM Trans. Graph., **27**, p. 65.

[55] Yuksel, C., Kaldor, J. M., James, D. L., and Marschner, S., 2012, "Stitch Meshes for Modeling Knitted Clothing With Yarn-Level Detail," ACM Trans. Graph., **31**(4), p. 37.

[56] Poincloux, S., Adda-Bedia, M., and Lechenault, F., 2018, "Geometry and Elasticity of a Knitted Fabric," Phys. Rev. X, **8**(2), p. 021075.

[57] Poincloux, S., Adda-Bedia, M., and Lechenault, F., 2018, "Crackling Dynamics in the Mechanical Response of Knitted Fabrics," Phys. Rev. Lett., **121**(5), p. 058002.

[58] Baraff, D., and Witkin, A., 1998, "Large Steps in Cloth Simulation," Proceedings of the 25th Annual Conference on Computer Graphics and Interactive Techniques, Orlando, FL, July 19–24, ACM, New York, pp. 43–54.

[59] Grinspun, E., Hirani, A. N., Desbrun, M., and Schröder, P., 2003, "Discrete Shells," Proceedings of the 2003 ACM SIGGRAPH/Eurographics Symposium on Computer Animation, San Diego, CA, July 26–27, Eurographics Association, pp. 62–67.

[60] Sharf, I., Thomsen, B., Botta, E. M., and Misra, A. K., 2017, "Experiments and Simulation of a Net Closing Mechanism for Tether-Net Capture of Space Debris," Acta Astronaut., **139**, pp. 332–343.

[61] Hou, Y., Liu, C., Hu, H., Yang, W., and Shi, J., 2021, "Dynamic Computation of a Tether-Net System Capturing a Space Target Via Discrete Elastic Rods and an Energy-Conserving Integrator," Acta Astronaut., **186**, pp. 118–134.

[62] Huang, W., and Jawed, M. K., 2019, "Newmark-Beta Method in Discrete Elastic Rods Algorithm to Avoid Energy Dissipation," ASME J. Appl. Mech., **86**(8), p. 084501.

[63] Huang, W., Wang, Y., Li, X., and Jawed, M. K., 2020, "Shear Induced Supercritical Pitchfork Bifurcation of Pre-Buckled Bands, From Narrow Strips to Wide Plates," J. Mech. Phys. Solids, **145**, p. 104168.

[64] Pérez, J., Thomaszewski, B., Coros, S., Bickel, B., Canabal, J. A., Sumner, R., and Otaduy, M. A., 2015, "Design and Fabrication of Flexible Rod Meshes," ACM Trans. Graph., **34**(4), p. 138.

[65] Sageman-Furnas, A. O., Chern, A., Ben-Chen, M., and Vaxman, A., 2019, "Chebyshev Nets From Commuting Polyvector Fields," ACM Trans. Graph., **38**(6), p. 172.